



HAL
open science

Combined US-ESR dating of fossil teeth from El Harhoura 2 cave (Morocco): New data about the end of the MSA in Temara region

Eslem Ben Arous, Christophe Falguères, Olivier Tombret, Mohamed Abdeljalil El Hajraoui, Roland Nespoulet

► To cite this version:

Eslem Ben Arous, Christophe Falguères, Olivier Tombret, Mohamed Abdeljalil El Hajraoui, Roland Nespoulet. Combined US-ESR dating of fossil teeth from El Harhoura 2 cave (Morocco): New data about the end of the MSA in Temara region. *Quaternary International*, 2020, 556, pp.88-95. 10.1016/j.quaint.2019.02.029 . hal-03015832

HAL Id: hal-03015832

<https://hal.science/hal-03015832>

Submitted on 20 Nov 2020

HAL is a multi-disciplinary open access archive for the deposit and dissemination of scientific research documents, whether they are published or not. The documents may come from teaching and research institutions in France or abroad, or from public or private research centers.

L'archive ouverte pluridisciplinaire **HAL**, est destinée au dépôt et à la diffusion de documents scientifiques de niveau recherche, publiés ou non, émanant des établissements d'enseignement et de recherche français ou étrangers, des laboratoires publics ou privés.

Accepted Manuscript

Combined US-ESR dating of fossil teeth from El Harhoura 2 cave (Morocco): New data about the end of the MSA in Temara region

Eslem Ben Arous, Christophe Falgueres, Olivier Tombret, Mohamed Abdeljalil El Hajraoui, Roland Nespoulet



PII: S1040-6182(18)31066-8

DOI: <https://doi.org/10.1016/j.quaint.2019.02.029>

Reference: JQI 7770

To appear in: *Quaternary International*

Received Date: 20 September 2018

Revised Date: 18 February 2019

Accepted Date: 19 February 2019

Please cite this article as: Ben Arous, E., Falgueres, C., Tombret, O., El Hajraoui, M.A., Nespoulet, R., Combined US-ESR dating of fossil teeth from El Harhoura 2 cave (Morocco): New data about the end of the MSA in Temara region, *Quaternary International* (2019), doi: <https://doi.org/10.1016/j.quaint.2019.02.029>.

This is a PDF file of an unedited manuscript that has been accepted for publication. As a service to our customers we are providing this early version of the manuscript. The manuscript will undergo copyediting, typesetting, and review of the resulting proof before it is published in its final form. Please note that during the production process errors may be discovered which could affect the content, and all legal disclaimers that apply to the journal pertain.

1 Combined US-ESR dating of fossil teeth from El Harhoura
2 cave (Morocco):
3 new data about the end of the MSA in Temara region.
4

5 Eslem BEN AROUS¹, Christophe FALGUERES¹, Olivier TOMBRET¹, Mohamed
6 Abdeljalil EL HAJRAOUI², Roland NESPOULET¹
7

8 ¹: UMR7194, Muséum national d'histoire naturelle, 1, rue René Panhard, 75013, Paris, France

9 ²: Institut National des Sciences de l'Archéologie et du Patrimoine, Rabat, Morocco
10

11 Corresponding author: E. Ben Arous

12 Email: eslem.ben-arous@mnhn.fr
13

14 **Abstract**

15 The study of the Middle Stone Age (MSA) in North Africa is essential to better understand
16 the human dispersals during the Late Pleistocene. The timing of the transition from the
17 MSA to the Later Stone Age (LSA) in the region is still debated due to the scarcity of sites
18 and the limited chronological constraints available. Among the few existing MIS 5 to MIS
19 1 archaeological sites in Northwestern Africa, El Harhoura 2 cave (Morocco) has been
20 extensively excavated during the last decade. It has provided MSA and LSA sequences
21 from which human remains have been systematically discovered in association with faunal
22 and lithic assemblages.

23 The combined US-ESR method has been applied to date five teeth from layer 3 and 4A,
24 which correspond to the most recent MSA occupations at El Harhoura 2 cave. The results
25 suggest the disappearance of the MSA at this site to have occurred around ~ 40 ka, at the
26 end of MIS 3, which is consistent with the palaeoenvironmental interpretation derived
27 from the faunal remains. These new results suggest that the last MSA human occupation
28 are ~15 ka more recent than previously showed by OSL dating. Further investigation is
29 required to fully understand the reason of such discrepancy between the two methods.
30

31 **1. Introduction**

32 During the last decades, research in Northwestern Africa has greatly improved the
33 chronology of the North Africa Middle Stone Age (Barton *et al.*, 2009, 2015; Dibble *et al.*,
34 2012; Doerschner *et al.*, 2016; El Hajraoui *et al.*, 2012; Jacobs *et al.*, 2011, 2012; Klasen *et al.*,
35 2017; Mercier *et al.*, 2007; Richter *et al.*, 2017, 2010; Schwenninger *et al.*, 2010).
36 These dating results have contributed to highlight the importance of this region in the study
37 of the origin and dispersal of anatomically modern humans within and out of Africa.

38 In North Africa, the end of the Late Pleistocene is marked by a cultural and subsistence
39 shift from the Middle Stone Age (MSA) to the Later Stone Age (LSA). The nature and
40 timing of this transition from MSA to LSA remains poorly known due to the paucity of
41 reliable dating data and a lack of well-stratified sites. This results in a large age uncertainty
42 for this transition, dated to between 60 and 25 ka.

43 El Harhoura 2 cave (Fig.1), located in Rabat-Temara region (Morocco), is one the few
44 sites in Northwestern Africa with a complete archeological sequence spanning from the
45 MSA and the Neolithic (El Hajraoui et al., 2012). This coastal area is well known for its
46 rich Middle to Late Pleistocene (MIS 5 to MIS 1) human fossil record. The MSA and LSA
47 human occupations are documented in Dar-es-Soltane 1, Dar-es-Soltane 2, El Harhoura 2,
48 El Mnasra and Contrebandiers caves. This area has also delivered most of MSA humans
49 remains (Debénath, 2000; El Hajraoui *et al.*, 2012). However, for some of the caves such
50 as El Mnasra, the stratigraphic interpretation of the deposits is complicated by post-
51 depositional perturbations (Lenoble, 2010). In contrast, the undisturbed archaeo-
52 stratigraphic record observed at El Harhoura 2 makes the site a good candidate to
53 chronologically constrain the disappearance of the MSA in the region.

54 In the present study, we applied the combined US-ESR dating method on
55 hydroxyapatite from herbivore fossil teeth (Grün *et al.*, 1988) to directly date human
56 occupation at El Harhoura 2. These results will contribute to the refine the end of the MSA
57 of Rabat-Temara sites.

58

59 **2. Geological, paleoenvironmental and archeological contexts**

60 El Hahroua 2 cave (33°57'08.9''N, 6°55'32.5''W) is located in Rabat-Temara region,
61 (Nespoulet et al., 2008; El Hajraoui et al., 2012). This karstic cave was dug in local
62 calcarenites by the marine erosion of the Plio-Pleistocene coastal ridge, described as a
63 succession of marine and continental deposits (Chahid *et al.*, 2016). Located 300 m from
64 the shoreline and 20.6 m above the present NGM (actual sea level), the site length is
65 estimated to 22 m, the depth around 9 m and the height ~ 8 m. El Harhoura 2 was
66 discovered in 1977 and a preliminary excavation was conducted mainly in the entrance
67 area (El Hajraoui et al. 2012). A first test pit of 8 m² was established in 1996, followed by
68 a lateral extension excavated in 2007, which allowed to describe the complete
69 archeological sequence at the entrance of the cave. In 2012, the excavation was further
70 extended to cover a total area of more than 200 m².

71 The sedimentary cave infilling is homogenous and dominated by sandy-clay matrix
72 (Boudad *et al.*, 2017). Four sedimentary units (Fig.2-A) were identified from bottom to
73 top. Unit I is dominated by grey sandy clays. Unit II is defined by a higher proportion of
74 clays and a lower content of silts. Unit III is described as an intermediate unit between clay
75 and carbonates and the Unit IV described by a lower content of sands.

76 Archeostratigraphy (Fig.2-A) has been mainly described from the test-pit of the
77 entrance area and subdivided into eleven levels (El Hajraoui et al., 2012). Level 1
78 (Neolithic), level 2 (LSA), levels 3, 4, 6, 8 (MSA). Other levels (5, 7, 9, 10 and 11) were
79 excavated only on a small surface (<3m²). For a total number of n=687 lithic artefacts
80 founded in the MSA levels, this number is less than n=14 for levels 5, 7, 9, 10 and 11 (El
81 Hajraoui et al., 2012, p.92). In the current state of excavations, these levels are considered
82 as archeologically sterile. Only the levels 3 and 4 are studied in this paper. The MSA
83 industries of these levels are composed by Levallois and micro-Levallois knapping tools,
84 laminar artifacts, side-scrapers and chopping tools. No tanged tools, characteristic of the
85 Aterian, have been recovered, even in extensively excavated areas. Humans burials were

86 found in the level 1 and 2 and post-cranial isolated bones were found on the levels 3 and 9
87 (El Hajraoui et al., 2012).

88 Taphonomic studies on abundant and well-preserved micro-faunal remains confirm
89 that no major disturbance occurred in these accumulations, and demonstrate the integrity of
90 the archeological levels (Stoetzel *et al.*, 2011). Zooarcheological studies (Campmas *et al.*,
91 2015) show a diversified faunal assemblage (presence of Alcelaphinae, Equidae, Bovinae
92 and Rhinocerotidae). Faunal spectrum is dominated by *Gazella* sp. which represent >70%
93 of the number of identified specimens (NISP) in levels 3 and 4A (and almost 57% in level
94 8). There is also a presence of carnivores (between 10% and 16% of the NISP for the levels
95 3 and 4A), which appear to be the main accumulators of large mammal remains in levels 2
96 to 5 (Campmas *et al.*, 2015). These observations, combined with results from the lithic
97 analysis (Stoetzel et al., 2014), show that human occupations in these levels were short and
98 non-intensive. Considering palaeoenvironmental reconstructions, both large and small
99 vertebrate assemblages from the whole archeological sequence show a succession of
100 relatively humid (levels 3, 4A, 6 and 8) and arid (levels 2, 5 and 7) phases (Stoetzel *et al.*,
101 2011, 2014).

102

103

104 **3. Material and methods**

105 Five fossil teeth (Fig.2-B-C) of *Equidae* (*Equus* sp.) and *Bovidae* (*Gazella* sp.) were
106 selected for dating analyses from the Institut National des Sciences de l'Archéologie et du
107 Patrimoine (INSAP, Rabat) collections (three from level 3, one near the limit between
108 levels 3 and 4A and one from level 4A). These teeth were collected during excavations
109 conducted between 2004 and 2010. Combined US-ESR dating analyses were performed at
110 the Geochronology laboratory of the Museum National d'Histoire Naturelle (MNHN) in
111 Paris.

112 Fossil teeth were prepared following the protocol described in Wagner et al. (2010).
113 Dental tissues (enamel, dentine, cement) were mechanically separated. Enamel samples
114 were cleaned using a dental drill then ground and sieved to 100-200 μm . Depending on the
115 amount of enamel powder available, each sample was split into 8, 9 or 10 aliquots (~50 mg
116 each) and irradiated using a ^{60}Co γ -ray source at LABRA (CEA, Saclay, France) in 2014.
117 ESR measurements were carried out at room temperature using EMX X-band Bruker
118 spectrometer and the following acquisition parameters: 5 scans, 1024 points resolution,
119 1.013 mW microwave power, 9.80 GHz microwave frequency, 100 kHz modulation
120 frequency, 0.1mT modulation amplitude, 20.48 ms conversion time and 5.12 ms time
121 constant. The ESR measurements were repeated 4 times for each aliquot over different
122 days. ESR intensities were extracted using the Bruker WINEPR System software from the
123 asymmetric ESR signal between the T1-B2 (Grün, 1998) and normalized by the weight of
124 each aliquot. Average ESR intensities from the repeated measurements were used for the
125 evaluation of the equivalent dose (D_e) determination.

126 D_e values (Table 1) were obtained by fitting a single saturated exponential (SSE)
127 function through the experimental data points (Yokoyama et al., 1985; Duval and Grün,
128 2016). Fitting was performed with Origin Pro8 software, with data weighted by the inverse
129 of the squared ESR intensity (Grün and Brumby, 1994). All ESR dose response curves are

130 provided in Fig.1 SM. An example of ESR spectrum is displayed in Fig.2 SM. This
131 spectrum shows a non-horizontal baseline which may potentially impact the D_e (Duval and
132 Martín-Francés, 2017). This was evaluated on one sample (EH2-2730) by performing a
133 baseline correction (using a cubic function) for each aliquot measured.

134 Alpha-ray spectrometry U-series analyses (Table 2) were carried out at the Musée de
135 l'Homme U-series laboratory. Samples (0.3-1 g) were dissolved in HNO_3 (7 N) and spiked
136 with ^{233}U , ^{236}U and ^{229}Th and charged onto anion exchange resin AG 1×8 (100-200 mesh
137 chloride form) in order to separate and purify U and Th sources (Shao et al., 2011). The
138 columns were rinsed with HCl (0.1 N) to collect uranium and purified using a UTEVA
139 resin column (Horwitz *et al.*, 1992) in HNO_3 (7 N). Th was eluted with HCl (8 N). The
140 purified U and Th were then evaporated by mixing TTA/benzene solution and deposited on
141 an iron disk covered by aluminum paper. Alpha counting was run for 8 days.

142 Dose rate provided on Table 1 was determined *in situ* (Table 3) using a γ -ray
143 portable spectrometer Inspector 1000 Canberra with NaI detector and following the
144 threshold technique (Mercier and Falguères, 2007). Additional high resolution γ -
145 spectroscopy measurements were performed at the Geochronology laboratory (Paris) on
146 raw sediment samples (Fig.2-C, Table SM.1), using a high resolution low-background Ge
147 detector, to determine the external β -dose rate from specific activity of U, Th, and K.
148 Analyses were performed on about 90 g of homogenized sediment samples sealed in a
149 plastic box during at least three weeks to ensure radon equilibrium.

150 The cosmic dose was evaluated according to Prescott and Hutton (1994). The
151 spatial configuration of the cave in different orientations (North, South, West and East)
152 was taken into account with a 3D model as in Richard et al. (2017).

153 Moisture content was measured in the laboratory by drying at 40°C for ten days.
154 The water content was estimated from the weight difference sediment before and after
155 drying. Sediments presented low water contents, below 5 %, which are quite similar to
156 values presented by Jacobs et al. (2012). However, we suspect these values may
157 underestimate the long-term water content, as sediment samples were collected in summer
158 (June 2014) in relatively dry conditions (archeological sections exposed to sunlight).
159 Consequently, we assumed instead a higher value of $10 \pm 5\%$ for age calculation (Grün,
160 1989).

161 Combined US-ESR ages were calculated using DATA program (Grün, 2009) and the
162 following parameters: α -efficiency of 0.13 ± 0.02 (Grün and Katzenberger-Apel, 1994), a
163 water content of 5 ± 3 wt% in dentine and cement and null in the enamel. β -attenuation
164 factors are from Brennan et al. (1997) and dose rate conversion factors from Guérin et al.,
165 (2011). Age results are given at 1σ confidence level. A cement/enamel/dentine
166 configuration was used for the age calculation of sample EH2-2993, whereas we used a
167 sediment/enamel/dentine configuration for the other samples.

168

169

170

171 **4. Results and discussion**

172

173 Equivalent doses, doses rates, p -values, and US-ESR ages calculated for each sample
174 are given in Table 1. U-series data and enamel thickness are presented in Table 2.

175 176 177 *U-series data*

178
179 Uranium content in the enamel ranges between 0.170 and 0.060 ppm, i.e. close to the
180 detection limits of α -ray spectrometry (see Falguères et al., 2018). U-content in cement and
181 dentine is between 4 and 8 ppm. $^{234}\text{U}/^{238}\text{U}$ ratios are systematically higher than 1 in dentine
182 and cement tissues. In enamel, this ratio is associated with large relative errors (between 10
183 and 20%), particularly for samples in which U content is very low. P -values for dental
184 tissues are superior than -1 and $^{230}\text{Th}/^{234}\text{U}$ values are lower than unity (between 0.03 and
185 0.81): they suggest that there is no uranium leaching in the dental tissues.

186 187 *Radioelements content*

188
189 Specific activities of ^{238}U , ^{226}Ra , ^{222}Rn and ^{232}Th in the surrounding sediments are
190 presented on Table SM.1. No significant disequilibrium in the U-238 decay chain is
191 observed for EH2-sed 1 and EH2-sed 2 sediments. In contrast, a 17 % loss of Ra and 26 %
192 of Rn-loss observed for EH2-sed 3 sample. The origin of these disequilibria is unknown.

193 194 195 *Equivalent doses*

196
197 D_e values range between 20 and 31 Gy. The ESR spectrum displayed in Fig.SM.2 of
198 the sample EH2-2730 presents a non-horizontal baseline. A sensitivity test performed on
199 sample EH2-2730 shows that baseline correction has, however, a very limited impact on
200 the D_e value (< 3 %). Following Duval and Grün (2016), the influence of the maximum
201 irradiation dose (D_{\max}) on the D_e estimate was also evaluated by successively removing the
202 last irradiation points (until 220-240 Gy). Results displayed in Fig.SM.4 show a minor
203 impact of D_{\max} in the present data set, as the difference between each resulting D_e does not
204 exceed the error range. Finally, repeated measurements ($n=4$) show relatively limited
205 variability of the individual D_e values derived from each independent measurement (<8%
206 for a given sample; Table SM.3). All these evidence consistently illustrate the robustness
207 of the ESR data set collected.

208 209 *Dose rate*

210
211 Results show that 3/4 teeth display homogeneous dose rates, except for EH2-2993
212 sample that exhibits a lower value by about 10%. This difference could be explained by the
213 presence in this tooth of a cement layer, which produced a lower β dose rate compared to
214 that from the surrounding sediment.

215 Gamma dose rates significantly contribute to the total dose rate by 50-60 % (Table 1,
216 Fig. SM.3), while cosmic dose rates represent 15-20% of the total dose rate. Consequently,

217 these two parameters significantly impact the age calculation. The correspondence between
218 sediment and *in situ* measurements with tooth samples is specified in table SM.1. The
219 comparison of our data with *in situ* gamma dose rates measured by Jacobs et al. (2012) and
220 those measured with TL-dosimeters by Janati-Idrissi et al., (2012) does not show
221 significant variability (Table 3). For level 3, values overall range from 368.3 ± 18.4 to
222 310.0 ± 15.5 $\mu\text{Gy/a}$. The present work and Jacobs et al. (2012) obtained mean values of
223 363.9 ± 18.2 and 346.7 ± 17.3 $\mu\text{Gy/a}$, respectively, which representing a variability $< 5\%$.
224 Similar observations can be made for level 4A: values range from 348.0 ± 17.4 to $385.4 \pm$
225 19.3 $\mu\text{Gy/a}$, with a variability of about 10% (Table 3). As these mean *in situ* gamma values
226 are very close to the individual *in situ* measurements, the latter were chosen to calculate
227 ages. To evaluate the potential impact of the moisture content on the calculated age,
228 simulations were performed by taking into account different moisture content ($3 \pm 1\%$, $5 \pm$
229 1% , $8 \pm 3\%$, $10 \pm 5\%$). Some of water content, as $3 \pm 1\%$, $5 \pm 1\%$, $6 \pm 2\%$, $7 \pm 2\%$ and $9 \pm$
230 2% have been used by Jacobs et al. (2012). Results are summarized on Fig.SM.5 and show
231 a difference of $< 1\%$. Consequently, whatever the water content used (between 3 and 10
232 %), the moisture content has virtually no impact on the calculated ages.

233

234

235 *Combined US-ESR ages*

236

237 Combined US-ESR range from 39 to 48 ka for the level 3 (with a mean age of $43.7 \pm$
238 4.5 ka) and from 46 to 49 ka for the level 4A.

239 EU-ESR ages, considered as minimum ages (Table SM.2), were also calculated using
240 DATA software for comparison. EU-ESR results are very close to US-ESR ages, with
241 differences ranging between 3 and 6 ka (between 7-15% of variability). This is due to the
242 fact that uranium content in dental tissue from El Harhoura 2 samples generated low dose
243 rate from teeth (accounting for 1-15 % of the total dose rate, Fig. 2 SM). Consequently, U-
244 uptake modelling has a negligible impact on the calculated ages, as often expected for Late
245 Pleistocene tooth samples (Richard, 2015). Combined US-ESR age results appear to be
246 overall stratigraphically consistent.

247

248

249 *Comparison with previous results*

250

251 Our ages are in agreement with previous combined US-ESR results obtained by Janati-
252 Idrissi et al. (2012) for the level 4A but they are younger than previous OSL dates. Only
253 two of OSL ages overlap with the combined US-ESR ages for the level 3 (Fig.3). Indeed,
254 OSL ages locating the age of the latest MSA human occupations around 57 ± 4 ka as a
255 mean age (Jacobs *et al.*, 2012) and the age of the level 4A at 74 ± 4 ka.

256 Regarding these data, the difference observed cannot be explained by the gamma dose
257 rates, which are quite similar for ESR and OSL samples. Considering the equivalent doses,
258 many remarks can be made. First of all, the D_e values determined using SG-SAR protocol
259 by Jacobs et al. (2012) lead to the identification of 2-3 quartz grain populations using
260 Finite Mixture Model (FMM). The presence of different components could be explained

261 either as mixing grains from underlying/overlying levels even if “mixing mechanism is not
262 clear”, or “by the effect of variations in the beta dose rate to individual grains” (Jacobs et
263 al., 2012, p.385-386). It is difficult to understand the meaning of these different population
264 grains in term of geology. In fact, the sedimentary processes in karstic coastal caves of this
265 area are not well understood in terms of chronology and origin, due to the impossibility to
266 differentiate quartz from different origins (aeolian, marine, peeling of the cave)(Niftah *et*
267 *al.*, 2005). The final OSL D_e chosen for age calculation correspond to the quartz grain
268 population statistically well represented (for level 3, between 63.7 ± 4.7 to $48.5 \pm 5\%$ of
269 representation). Consequently, the resulting OSL age estimates are about 20% higher than
270 our combined US-ESR ages. Using instead the D_e from the less representative quartz grain
271 population (between 5.0 ± 2.7 to $19.2 \pm 4.2\%$ of representation) would allow to recalculate
272 OSL ages between ~ 19 ka and 38 ka for level 3. For the level 4A, D_e from the less
273 representative quartz grain population ($8.7 \pm 3.7\%$ of representation) provides an OSL age
274 of about 42 ka. This result would be closer to the combined US-ESR ages.

275 The discrepancy of $\sim 20\%$ between previous OSL ages (Jacobs et al., 2012) and
276 combined US-ESR ages could also be explained by an underestimation of the D_e values
277 obtained for the fossil teeth, due to the presence of unstable radicals in the hydroxyapatite
278 as observed in Joannes-Boyau and Grün (2011) and Richter et al. (2017) on enamel
279 fragment. However, ESR dose estimate were carried out in the present study on enamel
280 powder, which results in randomly spatial distribution of the enamel crystals that renders
281 difficult such a comparison. The impact on these unstable components remains
282 nevertheless unclear and needs to be further investigated. It is indeed sample dependent,
283 and some teeth are simply not affected by this issue (e.g. Dirks *et al.*, 2017).

284 Combined US-ESR ages presented in this work suggest that the last MSA occupation
285 in Rabat-Temara is dated to around 40 ka. Other Northwestern African sites display similar
286 chronologies for late MSA occupations: ~ 29 ka using radiocarbon method in Taforalt
287 (Barton *et al.*, 2015) and 30.9 ± 2.5 ka with OSL (Weisrock *et al.*, 2008) for the end of
288 MSA without tanged tools at Wadi Noun.

289 In contrary, others sequences in the Rabat-Temara region show different chronologies:
290 for example, the latest MSA in Contrebandiers cave is older than 90 ka by OSL and 70 ka
291 by TL (Dibble *et al.*, 2012). However, erosion surface and the disruption in the deposits of
292 the Contrebandiers cave (Aldeias *et al.*, 2014) limit the discussion. Nevertheless, these
293 combined US-ESR of El Harhoura 2 cave match with previous TL ages obtained for
294 the end of MSA in El Harhoura 1 cave placed between 32.15 ± 4.8 ka and 41.16 ± 3.5 ka
295 (Debénath *et al.*, 1986).

296

297 5. Conclusion

298 The numerical ages obtained in the present study correlate the latest MSA human
299 occupations at El Harhoura 2 to the end of the MIS 3 (Fig.3). This attribution is in good
300 agreement with paleoenvironmental data derived from the study of micro fauna (Stoetzel
301 *et al.*, 2011), which position these levels in humid phase and associated to a tree-filled
302 meadow environment.

303 Combined US-ESR dating of fossil teeth provides a direct chronological constraint on
304 the archaeological levels at El Harhoura 2 and suggest that the latest MSA human

305 occupation may have occurred at least 15 ka after the OSL ages previously estimated by
306 Jacobs et al. (2012). The origin of the discrepancy between the results from the two
307 methods should however be further investigated in the future.

308 The direct dating of the last MSA human occupation at El Harhoura 2 cave provides an
309 important contribution to a better understanding of the timing of Late Pleistocene human
310 dispersals in the coastal environments of Northwestern Africa. Future investigations at
311 Rabat-Temara sites should focus on both the revision of old chronological data and new
312 dating application studies of well-identified and well-contextualized archeological material
313 in order to improve the existing chronological framework of the area.

314

315

316 **Acknowledgements**

317 Authors thank to A. Akerraz, director of INSAP, for access to the faunal collections
318 from EL Harhoura 2 in 2014. We also thank J.-J. Bahain and E. Stoetzel for their
319 constructive helpful discussion/advices. The authors are grateful to three anonymous
320 reviewers for constructive and useful comments on an earlier version of this article.

321

322 **References**

323

324 Aldeias V, Goldberg P, Dibble HL and El-Hajraoui M, 2014, Deciphering site formation
325 processes through soil micromorphology at Contrebandiers Cave, Morocco. *Journal of*
326 *Human Evolution*. Elsevier Ltd 69(1): 8–30, DOI: 10.1016/j.jhevol.2013.12.016.

327 Barton RNE, Bouzouggar A, Collcutt SN, Carrión Marco Y, Clark-Balzan L, Debenham
328 NC and Morales J, 2015, Reconsidering the MSA to LSA transition at Taforalt Cave
329 (Morocco) in the light of new multi-proxy dating evidence. *Quaternary International* 1–
330 14, DOI: 10.1016/j.quaint.2015.11.085.

331 Barton RNE, Bouzouggar A, Collcutt SN, Schwenninger JL and Clark-Balzan L, 2009,
332 OSL dating of the Aterian levels at Dar es-Soltan I (Rabat, Morocco) and implications for
333 the dispersal of modern Homo sapiens. *Quaternary Science Reviews*. Elsevier Ltd 28(19–
334 20): 1914–1931, DOI: 10.1016/j.quascirev.2009.03.010.

335 Boudad L, El Hammouti K, Chahid D, Nespoulet R and El Hajraoui A, 2017, Les indices
336 climatiques du Pléistocène supérieur et de l'Holocène des formations quaternaires de la
337 côte atlantique (Rabat-Témara, Maroc). *Anthropologie (France)*. Elsevier Masson SAS
338 121(1–2): 90–101, DOI: 10.1016/j.anthro.2017.03.007.

339 Brennan BJ, Rink WJ, McGuirl EL, Schwarcz HP and Prestwich WV, 1997, Beta doses in
340 tooth enamel by “one-group” theory and the ROSY ESR dating software. *Radiation*
341 *Measurements*. Pergamon 27(2): 307–314, DOI: 10.1016/S1350-4487(96)00132-1.

342 Campmas E, Michel P, Costamagno S, Amani F, Stoetzel E, Nespoulet R and El Hajraoui
343 MA, 2015, Were Upper Pleistocene human/non-human predator occupations at the Témara
344 caves (El Harhoura 2 and El Mnasra, Morocco) influenced by climate change? *Journal of*
345 *Human Evolution*. Elsevier Ltd 78: 122–143, DOI: 10.1016/j.jhevol.2014.08.008.

346 Chahid D, Boudad L, Lenoble A, Hmadi A El, Chakroun A and Jacobs Z, 2016,
347 Nouvelles données morpho-stratigraphiques et géochronologiques sur le cordon littoral
348 externe (SIM 5-c) de Rabat – Témara , Maroc. *Géomorphologie : relief, processus*,

- 349 *environnement.*
- 350 Debénath A, 2000, Le peuplement préhistorique du Maroc: données récentes et problèmes.
351 *L'anthropologie* 104: 131–145, DOI: 10.1016/S0003-5521(00)90006-2.
- 352 Debénath A, Raynal J-P, Roche J, Texier JP and Ferembach D, 1986, Stratigraphie,
353 habitat, typologie et devenir de l'Atérien marocain : données récentes. *L'anthropologie*
354 90(2): 233–246.
- 355 Dibble HL, Ández EA, Blackwell BAB, Hallett-desguez E, Lin SAMC, Meyer MC and
356 Steele TE, 2012, New Excavations at the Site of Contrebandiers Cave, Morocco.
357 *PaleoAnthropology* 145–201, DOI: 10.4207/PA.2012.ART74.
- 358 Dirks PH, Roberts EM, Hilbert-Wolf H, Kramers JD, Hawks J, Dosseto A, Duval M,
359 Elliott M, Evans M, Grün R, Hellstrom J, Herries AI, Joannes-Boyau R, Makhubela T V,
360 Placzek CJ, Robbins J, Spandler C, Wiersma J, Woodhead J and Berger LR, 2017, The age
361 of Homo naledi and associated sediments in the Rising Star Cave, South Africa. *eLife* 6,
362 DOI: 10.7554/eLife.24231.
- 363 Doerschner N, Fitzsimmons KE, Ditchfield P, McLaren SJ, Steele TE, Zielhofer C,
364 McPherron SP, Bouzouggar A and Hublin J-J, 2016, A New Chronology for Rhafas,
365 Northeast Morocco, Spanning the North African Middle Stone Age through to the
366 Neolithic. *Plos One* 11(9): e0162280, DOI: 10.1371/journal.pone.0162280.
- 367 Duval M and Grün R, 2016, Are published ESR dose assessments on fossil tooth enamel
368 reliable? *Quaternary Geochronology* 31: 19–27, DOI: 10.1016/j.quageo.2015.09.007.
- 369 Duval M and Martín-Francés L, 2017, Quantifying the impact of μ CT-scanning of human
370 fossil teeth on ESR age results. *American Journal of Physical Anthropology*. John Wiley &
371 Sons, Ltd 163(1): 205–212, DOI: 10.1002/ajpa.23180.
- 372 El Hajraoui MA, Nespoulet R, Debénath A and Dibble H, 2012, *Préhistoire de la région*
373 *de Rabat-Témara.*
- 374 Falguères C, Ghaleb B, Tombret O, Ben Arous E, Richard M, Moigne AM, Saos T, Frouin
375 M, Caparros M and Barroso-Ruiz C, 2018, ESR/U-series dates on Equus teeth from the
376 Middle Pleistocene Acheulean site of Cueva del Angel, Spain. *Quaternary Geochronology*.
377 Elsevier, DOI: 10.1016/J.QUAGEO.2018.02.003.
- 378 Grün R, 1989, Electron spin resonance (ESR) dating. *Quaternary International* (1): 65–
379 109.
- 380 Grün R, 1998, *Reproducibility measurements for ESR signal intensity and dose*
381 *determination: High precision but doubtful accuracy.* *Radiation Measurements*, DOI:
382 10.1016/S1350-4487(98)00014-6.
- 383 Grün R, 2009, The relevance of parametric U-uptake models in ESR age calculations.
384 *Radiation Measurements*. Elsevier Ltd 44(5–6): 472–476, DOI:
385 10.1016/j.radmeas.2009.02.011.
- 386 Grün R and Brumby S, 1994, The assessment of errors in past radiation doses extrapolated
387 from ESR/TL dose-response data. *Radiation Measurements* 23: 307–315.
- 388 Grün R and Katzenberger-Apel O, 1994, An alpha-irradiator for ESR dating. *Ancient TL*
389 (12): 35–38.
- 390 Grün R, Schwarcz HP and Chadam J, 1988, ESR dating of tooth enamel: Coupled

- 391 correction for U-uptake and U-series disequilibrium. *International Journal of Radiation*
392 *Applications and Instrumentation. Part 14*(1–2): 237–241, DOI: 10.1016/1359-
393 0189(88)90071-4.
- 394 Guérin G, Mercier N and Adamiec G, 2011, Dose-rate conversion factor: update. *Ancient*
395 *TL* 29(1): 5–8.
- 396 Horwitz EP, Dietz ML, Rhoads SM, Chiarizian R, Diamond H, Essling AM and Graczyk
397 D, 1992, Separation and preconcentration of lead from acidic media by extraction
398 chromatography. *Analytica Chimica Acta* 266: 25–37.
- 399 Jacobs Z, Meyer MC, Roberts RG, Aldeias V, Dibble H and El Hajraoui MA, 2011,
400 Single-grain OSL dating at La Grotte des Contrebandiers (“Smugglers” Cave’), Morocco:
401 Improved age constraints for the Middle Paleolithic levels. *Journal of Archaeological*
402 *Science*. Elsevier Ltd 38(12): 3631–3643, DOI: 10.1016/j.jas.2011.08.033.
- 403 Jacobs Z, Roberts RG, Nespoulet R, El Hajraoui MA and Debénath A, 2012, Single-grain
404 OSL chronologies for Middle Palaeolithic deposits at El Mnasra and El Harhoura 2,
405 Morocco: Implications for Late Pleistocene human-environment interactions along the
406 Atlantic coast of northwest Africa. *Journal of Human Evolution* 62(3): 377–394, DOI:
407 10.1016/j.jhevol.2011.12.001.
- 408 Janati-Idrissi N, Falguères C, Haddad M, Nespoulet R, Abdeljalil M, Hajraoui EL,
409 Debénath A, Bejjit L, Bahain J, Michel P, Garcia T, Boudad L, Hammouti K El and Oujaa
410 A, 2012, Datation Par ESR-U/Th combinées de dents fossiles des Grottes d’El Mnasra et
411 D’ El Harhoura 2 , région de Rabat-Témara. Implications chronologiques sur le
412 peuplement du Maroc Atlantique au Pléistocène Supérieur et son environnement.
413 *Quaternaire* 23(1): 25–35.
- 414 Joannes-Boyau R and Grün R, 2011, A comprehensive model for CO₂– radicals in fossil
415 tooth enamel: Implications for ESR dating. *Quaternary Geochronology*. Elsevier 6(1): 82–
416 97, DOI: 10.1016/J.QUAGEO.2010.09.001.
- 417 Klasen N, Kehl M, Mikdad A, Brückner H and Weniger G-C, 2017, Chronology and
418 formation processes of the Middle to Upper Palaeolithic deposits of Ifri n’Ammar using
419 multi-method luminescence dating and micromorphology. *Quaternary International*.
420 Elsevier Ltd and INQUA 1–14, DOI: 10.1016/j.quaint.2017.10.043.
- 421 Lenoble, A., 2010. Lithostratigraphie de la grotte d’El Mnasra. Description et hypothèses
422 proposées. In: El Hajraoui, M.A., Nespoulet, R. (Eds.), Mission Archéologique El
423 Harhoura-Témara, pp. 14e15. Programme de coopération: Ministère de la Culture (Rabat),
424 Ministère des Affaires Etrangères et Européennes (Paris), Unpublished.
- 425 Lisiecki LE and Raymo ME, 2005, A Pliocene-Pleistocene stack of 57 globally distributed
426 benthic $\delta^{18}O$ records. *Paleoceanography* 20(1): 1–17, DOI: 10.1029/2004PA001071.
- 427 Mercier N and Falguères C, 2007, Field gamma dose-rate measurement with a NaI(Tl)
428 detector: re-evaluation of the “threshold” technique. *Ancient TL* 25(1): 1–4.
- 429 Mercier N, Wengler L, Valladas H, Joron JL, Froget L and Reyss JL, 2007, The Rhafas
430 Cave (Morocco): Chronology of the mousterian and atherian archaeological occupations and
431 their implications for Quaternary geochronology based on luminescence (TL/OSL) age
432 determinations. *Quaternary Geochronology* 2(1–4): 309–313, DOI:
433 10.1016/j.quageo.2006.03.010.

- 434 Nespoulet R, El Hajraoui MA, Amani F, Ben Ncer A, Debénath A, Idrissi A, Lacombe JP,
435 Michel P, Oujaa A and Stoetzel E, 2008, Palaeolithic and neolithic occupations in the
436 Témara region (Rabat, Morocco): Recent data on hominin contexts and behavior. *African*
437 *Archaeological Review* 25(1–2): 21–39, DOI: 10.1007/s10437-008-9025-1.
- 438 Niftah S, Debénath A and Miskovsky J-C, 2005, Origine du remplissage sédimentaire des
439 grottes de Témara (Maroc) d’après l’étude des minéraux lourds et l’étude exoscopique des
440 grains de quartz. *Quaternaire* 16(2): 73–83.
- 441 Prescott JR and Hutton JT, 1994, Cosmic ray contributions to dose rates for luminescence
442 and ESR dating: Large depths and long-term time variations. *Radiation Measurements*.
443 Pergamon 23(2–3): 497–500, DOI: 10.1016/1350-4487(94)90086-8.
- 444 Richard M, 2015, Chronologie des occupations humaines au Pléistocène supérieur dans le
445 Jura Souabe , Allemagne et dans les vallées de la Saône et du Rhône, France, par les
446 méthodes de la résonance de spin électronique et des séries de l’ uranium, ESR / U-Th.
- 447 Richter D, Grün R, Joannes-Boyau R, Steele TE, Amani F, Rué M, Fernandes P, Raynal J-
448 P, Geraads D, Ben-Ncer A, Hublin J-J and McPherron SP, 2017, The age of the hominin
449 fossils from Jebel Irhoud, Morocco, and the origins of the Middle Stone Age. *Nature*
450 546(7657): 293–296, DOI: 10.1038/nature22335.
- 451 Richter D, Moser J, Nami M, Eiwanger J and Mikdad A, 2010, New chronometric data
452 from Ifri n’ Ammar (Morocco) and the chronostratigraphy of the Middle Palaeolithic in the
453 Western Maghreb. *Journal of Human Evolution*. Elsevier Ltd 59(6): 672–679, DOI:
454 10.1016/j.jhevol.2010.07.024.
- 455 Schwenninger J-L, Collcutt SN, Barton N, Bouzouggar A, Clark-Balzan L, El Hajraoui
456 MA, Nespoulet R and Debénath A, 2010, A New Luminescence Chronology for Aterian
457 Cave Sites on the Atlantic Coast of Morocco. In: Garc (ed) *South-Eastern Mediterranean*
458 *Peoples Between 130, 000 and 10, 000 Years Ago*, 18–36.
- 459 Shao Q, Bahain J-J, Falguères C, Peretto C, Arzarello M, Minelli A, Thun Hohenstein U,
460 Dolo J-M, Garcia T, Frank N and Douville E, 2011, New ESR/U-series data for the early
461 Middle Pleistocene site of Isernia la Pineta, Italy. *Radiation Measurements*. Pergamon
462 46(9): 847–852, DOI: 10.1016/J.RADMEAS.2011.03.026.
- 463 Stoetzel E, Campmas E, Michel P, Bougariane B, Ouchaou B, Amani F, El Hajraoui MA
464 and Nespoulet R, 2014, Context of modern human occupations in North Africa:
465 Contribution of the Témara caves data. *Quaternary International*. Elsevier Ltd and
466 INQUA 320: 143–161, DOI: 10.1016/j.quaint.2013.05.017.
- 467 Stoetzel E, Marion L, Nespoulet R, El Hajraoui MA and Denys C, 2011, Taphonomy and
468 palaeoecology of the late Pleistocene to middle Holocene small mammal succession of El
469 Harhoura 2 cave (Rabat-Témara, Morocco). *Journal of human evolution* 60(1): 1–33, DOI:
470 10.1016/j.jhevol.2010.07.016.
- 471 Wagner GA, Krbetschek M, Degering D, Bahain J-J, Shao Q, Falgueres C, Voinchet P,
472 Dolo J-M, Garcia T and Rightmire GP, 2010, Radiometric dating of the type-site for Homo
473 heidelbergensis at Mauer, Germany. *Proceedings of the National Academy of Sciences*
474 107(46): 19726–19730, DOI: 10.1073/pnas.1012722107.
- 475 Weisrock A, Rousseau L, Reyss JL, Falguères C, Ghaleb B, Bahain JJ, Beauchamp J,
476 Boudad L, Mercier N, Mahieux G, Pozzi JP, Janati-Idrissi N and Ouammou A, 2008,
477 Travertins de la bordure nord du Sahara Marocain: Dispositifs morphologiques, datations

478 U/Th et indications paléoclimatiques. *Geomorphologie: Relief, Processus, Environnement*
479 (3): 153–168, DOI: 10.4000/geomorphologie.6793.

480 Yokoyama Y, Falguères C and Quaegebeur JP, 1985, ESR dating of quartz from
481 Quaternary sediments : first attempts. *Nuclear Tracks* (10): 921–928.

482

483

484 **Figure captions**

485

486 Figure 1: Location of El Harhoura 2 cave in Rabat-Temara region, Northwestern Africa
487 (Map modified from El Hajraoui *et al.*, 2012).

488

489 Figure 2: Synthetic stratigraphy (A) of the El Harhoura 2 site (modified from El Hajraoui
490 *et al.*, 2012), including the location of the relative area where the sediments and tooth
491 samples come from (B), their depth distribution projected on the North-South profile (C).
492 Photo: R. Nespoulet and C. Falguères.

493

494 Figure 3: Synthesis of the US-ESR and OSL ages obtained for the level 3 and 4A opposite to
495 the $\delta^{18}\text{O}$ data from Lisiecki and Raymo (2005).

496

497

498 **Table captions**

499

500 Table 1: Equivalent dose (D_e), Dose rate and combined US-ESR age estimation presented
501 at 1 σ confidence level. Key: e= enamel; d=dentine; c=cement. The dose rate components
502 presented are: internal dose rate ($\alpha + \beta$ of the enamel), β_1 (beta contribution from the
503 dentine), β_2 (beta contribution from cement or sediment), gamma and cosmic dose rates.

504

505 Table 2: U-series data obtained by alpha-spectrometry analyses of El Harhoura 2 tooth
506 samples. Data are presented with 2 σ . Key: D= dentine; C= cement; E = enamel; side 1
507 =dentine and side 2 =sediment or cement. For enamel in low U-content, isotopic ratios
508 (italic) are associated with large relative errors (between 10 and 20%).

509

510 Table 3: *In situ* gamma dosimetry measured with a NaI detector (Jacobs *et al.*, 2012; this
511 work) and TL dosimeters (Janati-Idrissi *et al.*, 2012) in levels 3 and 4A. A mean value was
512 calculated for each level. Error associated to mean value is the mean of error. A 5% error
513 was assumed for each individual measurement. For level 3, 5 % variability was estimated
514 from the two mean values (346.7 ± 17.3 and 363.9 ± 18.2). For level 4A, 10 % variability
515 was estimated from the two values presented (370.0 ± 18.5 and 348.0 ± 17.4); *: initial
516 value given was 438 $\mu\text{Gy/a}$ and the cosmic dose rate of 90 $\mu\text{Gy/a}$ was subtracted from this
517 value.

518

519

520
521
522
523
524
525
526
527

528 **Supplementary material**

529

530 Table SM.1: ^{238}U , ^{226}Ra , ^{222}Rn , ^{232}Th and ^{40}K content (dpm/g or %) measured and
531 converted using dose rate factors published in Guérin *et al.* (2011). Sample EH2-sed 3 has
532 been measured but not used on this calculation because of its geographical distance from
533 the teeth samples.

534

535 Table SM.2: EU-ESR and combined US-ESR ages comparison for tooth samples dated in
536 this work. Errors are displayed at 1σ .

537

538 Table SM.3: D_e values over the repeated ESR measurements ($n=4$). The dispersion of the
539 individual D_e per sample is not significantly important and remains rarely more than $\sim 8\%$ ($<$
540 3 Gy). RSD: relative standard deviation. Data are associated with 1σ .

541

542 Figure SM.1: ESR dose response curve for samples dated in this work computing by
543 Origin Pro 8 software, using SSE function (Yokoyama *et al.*, 1985; Duval and Grün,
544 2016). All D_e presented range between 20 and 31 Gy.

545

546 Figure SM.2: ESR spectra measured in sample EH2-2730.

547

548 Figure SM.3: proportion of the different dose rate components. Key: I_{internal} = dose rate α
549 + β contribution from the enamel, β_1 = beta contribution from the dentine, β_2 = beta
550 contribution from cement or sediment.

551

552 Figure SM.4: Evolution of D_e as a function of D_{max} for all samples fitted with a SSE
553 function. 1σ errors are displayed. The D_e value used for the US-ESR calculation is shown
554 with a dash line.

555

556 Figure SM.5: recalculated combined US-ESR ages in taking account different water
557 content of $3 \pm 1\%$, $5 \pm 1\%$, $8 \pm 3\%$ and $10 \pm 5\%$.

Sample	Sample Level	Dose rate (Gy)		Z (cm)	Tissue	U-content (ppm)				Dose rate ($\mu\text{Gy/a}$)				Initial enamel thickness (μm)		Enamel removed side 1 (μm)		Enamel removed side 2 (μm)		Uptake parameter (p-values)	
						\pm Internal ($\alpha + \beta$)	\pm $\beta 1$	\pm $\beta 2$	\pm Gamma	\pm Cosmic	\pm Total	\pm US-ESR	\pm Age								e
EH2-2993	3	19.95	0.8	7	2	16	4	11	2	378	27	104	10	516	27	39	3	1.27 \pm 0.33	0.58 \pm 0.39	1.27 \pm 0.33	
EH2-3986	3	27.25	3.8	11	5	50	22	91	8	362	36	104	10	618	43	44	7	-0.64 \pm 0.1	-0.43 \pm 0.21	-	
EH2-2730	3	28.83	0.8	0	0	26	6	108	10	368	39	104	10	606	41	48	4	19.56 \pm 2.02	0.72 \pm 0.38	-	
EH2-10221	4A	30.19	1.7	17	14	30	6	90	9	389	22	93	10	619	31	49	5	-0.87 \pm 0.09	0 \pm 0.20	-	
EH2-10984	4A	29.13	1.1	12	5	50	7	103	11	372	27	93	10	630	33	46	3	-0.74 \pm 0.15	-0.22 \pm 0.10	-	

Table 1: Equivalent dose (D_e), Dose rate and combined US-ESR age estimation presented at 1 σ confidence level. Key: e= enamel; d=dentine; c=cement. The dose rate components presented are: internal dose rate ($\alpha + \beta$ of the enamel), $\beta 1$ (beta contribution from the dentine), $\beta 2$ (beta contribution from cement or sediment), gamma and cosmic dose rates.

<i>EH2-2993</i>	3	-415	D	4.72	0.17	1.05	0.04	0.13	0.01	830 ± 83	39 ± 4	57 ± 6
			C	4.78	0.22	1.14	0.06	0.03	0.03			
			E	0.17	0.02	<i>0.94</i>	<i>0.14</i>	<i>0.09</i>	<i>0.09</i>			
<i>EH2-3986</i>	3	-426	D	7.90	0.47	1.05	0.06	0.29	0.06	720 ± 72	43 ± 4	94 ± 9
			E	0.06	0.01	<i>0.90</i>	<i>0.21</i>	<i>0.25</i>	<i>0.82</i>			
<i>EH2-2730</i>	3	-437	D	7.44	0.44	1.06	0.06	0.14	0.02	690 ± 69	53 ± 5	40 ± 5
			E	0.07	0.01	1.29	0.26	<i>0.03</i>	<i>0.16</i>			
<i>EH2-10221</i>	4A	-458	D	6.59	0.29	1.05	0.05	0.75	0.17	710 ± 71	92 ± 9	64 ± 6
			E	0.15	0.04	1.05	0.35	0.81	0.32			
<i>EH2-10984</i>	4A	-470	D	7.98	0.31	1.16	0.05	0.18	0.02	700 ± 70	58 ± 6	54 ± 5
			E	0.09	0.02	<i>0.72</i>	<i>0.24</i>	<i>0.67</i>	<i>0.38</i>			

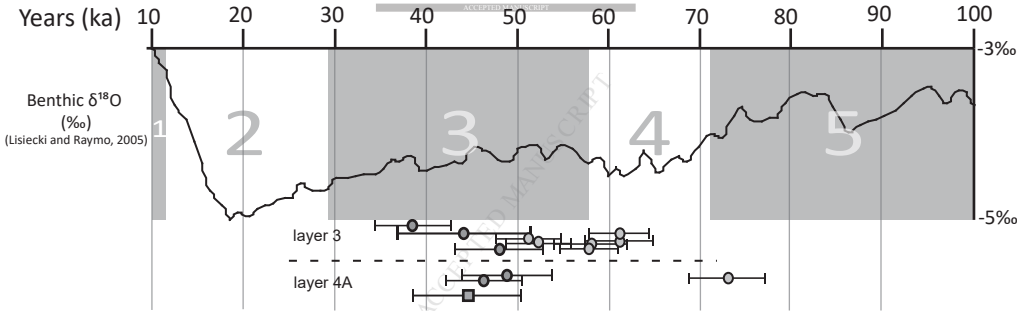
Table 2: U-series data obtained by alpha-spectrometry analyses of El Harhoura 2 tooth samples. Data are presented with 2σ . Key: D= dentine; C= cement; E = enamel; side 1 =dentine and side 2 =sediment or cement. For enamel in low U-content, isotopic ratios (italic) are associated with large relative errors (between 10 and 20%).

Gamma Dose rate ($\mu\text{Gy/a}$)

Layer	This work	Jacobs et al., 2012	Janati-Idrissi et al., 2012	% Variability
-------	-----------	---------------------	-----------------------------	---------------

3		\pm		\pm	5
	(dos 34)		310.0	15.5	
	368.3	18.4	360.0	18.0	
	(dos 35)		370.0	18.5	
	359.4	18.0	350.0	17.5	
	(dos 36)		350.0	17.5	
			340.0	17.0	
	Mean	363.9	18.2	346.7	17.3
4A	(dos 33)		370.0	18.5	10
	385.4	19.3	348.0*	17.4	
	Mean		367.8	18.8	

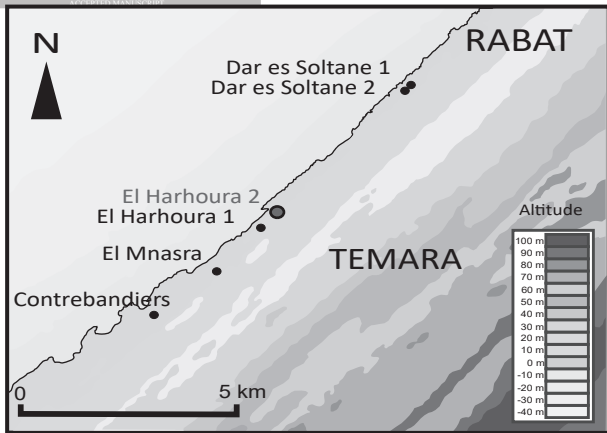
Table 3: *In situ* gamma dosimetry measured with a NaI detector (Jacobs *et al.*, 2012; this work) and TL dosimeters (Janati-Idrissi *et al.*, 2012) in levels 3 and 4A. A mean value was calculated for each level. Error associated to mean value is the mean of error. A 5% error was assumed for each individual measurement. For level 3, 5 % variability was estimated from the two mean values (346.7 ± 17.3 and 363.9 ± 18.2). For level 4A, 10 % variability was estimated from the two values presented (370.0 ± 18.5 and 348.0 ± 17.4); *: initial value given was $438 \mu\text{Gy/a}$ and the cosmic dose rate of $90 \mu\text{Gy/a}$ was subtracted from this value.

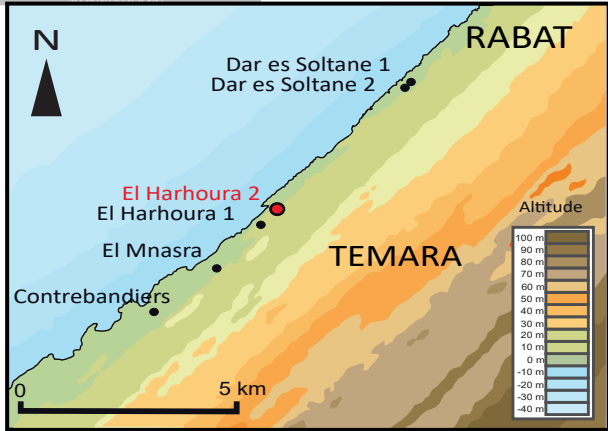


● ESR/U-series ages (this work)

○ SG-OSL ages (Jacobs et al., 2012)

■ ESR/U-series ages (Janati-Idrissi et al., 2012)





A

El Harhoura 2

Archeostratigraphy

Sedimentology

Neolithic

1

I

Later Stone Age

2

3

II

4A

4B

Middle Stone Age

5

6

7

8

9

10

11


III

IV

Area not excavated

1 m

Legend

-  powdered ashy layer
-  yellowish sandy-clay
-  brown red sandy-clay
-  brown grey sandy-clay
-  brown reddish sandy-clay
-  brown yellowish sandy-clay
-  brown red sandy-clay
-  brown reddish sandy-clay
-  limestone
-  manganese
-  ash

A

El Harhoura 2

Archeostratigraphy

Sedimentology

Neolithic

1

I

Later Stone Age

2

3

II

4A

4B

Middle Stone Age

5

6

7

8

9

10

11

IV

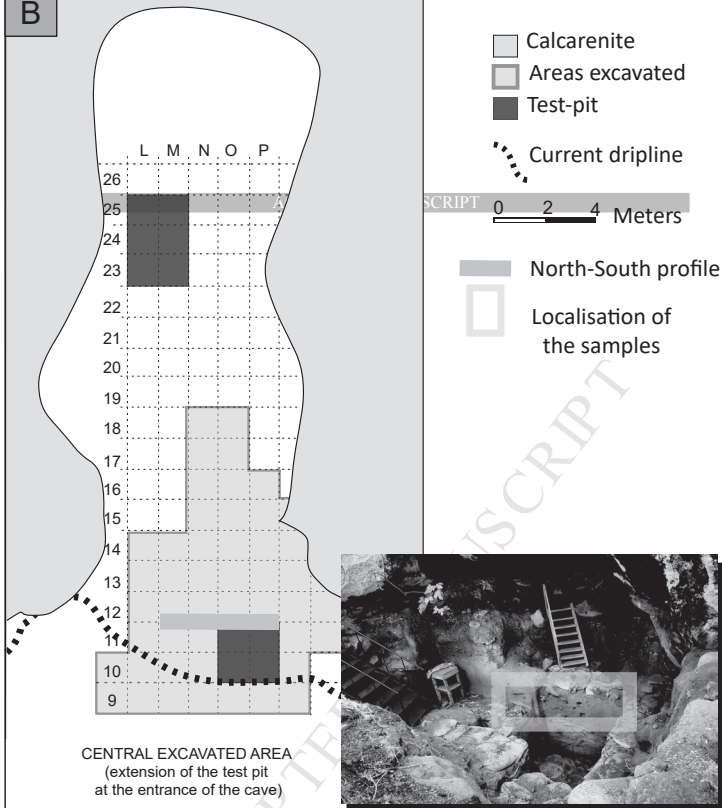
Area not
excavated

1 m

Legend

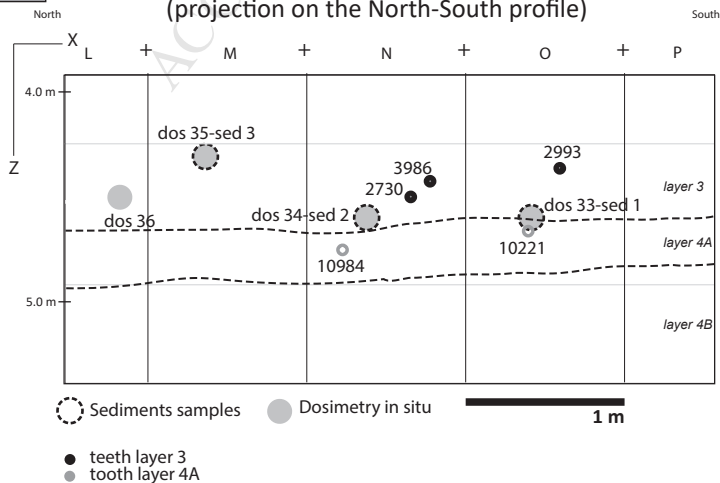
-  powdered ashy layer
-  yellowish sandy-clay
-  brown red sandy-clay
-  brown grey sandy-clay
-  brown reddish sandy-clay
-  brown yellowish sandy-clay
-  brown red sandy-clay
-  brown reddish sandy-clay
-  limestone
-  manganese
-  ash

B

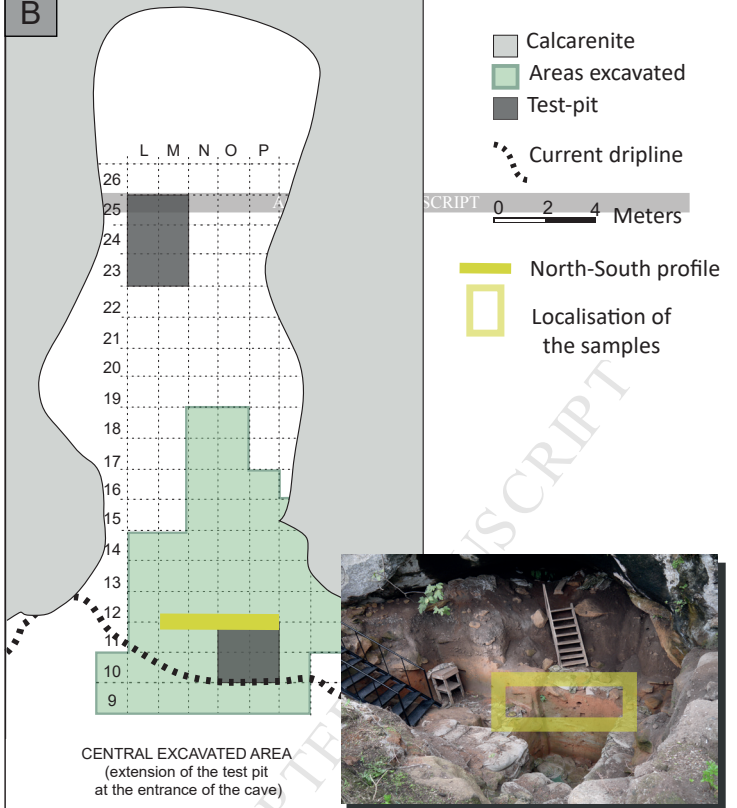


C

Repartition of the samples (projection on the North-South profile)



B



C

Repartition of the samples (projection on the North-South profile)

